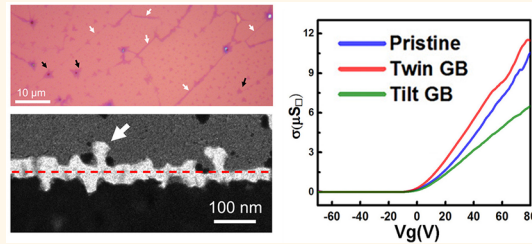


Electrical Transport Properties of Polycrystalline Monolayer Molybdenum Disulfide

Sina Najmaei,^{†,§} Matin Amani,^{‡,§} Matthew L. Chin,[‡] Zheng Liu,^{†,||,¶} A. Glen Birdwell,[‡] Terrance P. O'Regan,[‡] Pulickel M. Ajayan,[†] Madan Dubey,^{‡,*} and Jun Lou^{†,*}

[†]Department of Materials Science and NanoEngineering, Rice University, Houston, Texas 77005, United States and [‡]Sensors and Electron Devices Directorate, US Army Research Laboratory, Adelphi, Maryland 20723, United States. [§]These authors contributed equally. ^{||}Present address: School of Materials Science and Engineering, Nanyang Technological University, 639798, Singapore. [¶]Present address: NOVITAS, Nanoelectronics Centre of Excellence, School of Electrical and Electronic Engineering, Nanyang Technological University, 639798, Singapore.

ABSTRACT Semiconducting MoS₂ monolayers have shown many promising electrical properties, and the inevitable polycrystallinity in synthetic, large-area films renders understanding the effect of structural defects, such as grain boundaries (GBs, or line-defects in two-dimensional materials), essential. In this work, we first examine the role of GBs in the electrical-transport properties of MoS₂ monolayers with varying line-defect densities. We reveal a systematic degradation of electrical characteristics as the line-defect density increases. The two common MoS₂ GB types and their specific roles are further examined, and we find that only tilt GBs have a considerable effect on the MoS₂ electrical properties. By examining the electronic states and sources of disorder using temperature-dependent transport studies, we adopt the Anderson model for disordered systems to explain the observed transport behaviors in different temperature regimes. Our results elucidate the roles played by GBs in different scenarios and give insights into their underlying scattering mechanisms.



KEYWORDS: two-dimensional materials · MoS₂ · polycrystallinity · grain boundaries · electronic transport

The existence of an intrinsic direct band gap and the fascinating physics of two-dimensional (2D) MoS₂ have led to intensive studies of this material in the past few years.^{1–7} This effort has been greatly facilitated by the development of new MoS₂ synthetic approaches.^{8–12} The introduction of a large number and diverse types of defects into the crystal structure of this material is a natural consequence of chemical growth.^{11–14} Therefore, understanding the nature of these disorders and their roles in the physical properties of MoS₂ is essential for its future development. A grain boundary (GB), a prominent type of defect in chemical vapor deposition (CVD)-grown MoS₂, is a one-dimensional (1D) line defect in the 2D lattice and mediates the transition from one crystalline orientation to another. Previous research on the role of grain boundaries (GBs) in the transport properties of 2D materials shows considerable diversity.^{14–18} The theoretical examination of their roles in graphene predicts two

distinct behaviors based on different grain boundary structures.¹⁵ Li *et al.* demonstrated the collective role of grain boundaries in the transport properties of graphene by controlling the grain size from 6 to 20 μm.¹⁷ These results show that the charge carrier mobility of the samples decreases roughly by 2-fold as the grain sizes decrease in this range. Additional experiments on graphene samples synthesized through different synthetic routes suggest that sample preparation may play an even more important role in electron transport behaviors across grain boundaries.¹⁸ These results show that growth conditions may dominate the quality of grain boundaries formed. For instance, slower graphene growth results in larger grain sizes; however, the layers are often discontinuous across grain boundaries. For this reason, electron transport across grains made from this growth process show higher degradation in transport properties of graphene.

The polycrystalline MoS₂ films show similar complexity in GB structures, and different forms of line-defects have been

* Address correspondence to jlou@rice.edu.

Received for review March 27, 2014 and accepted July 14, 2014.

Published online July 14, 2014
10.1021/nn501701a

© 2014 American Chemical Society

observed.^{11–14} It has been shown that, in addition to conventional GBs, bilayer growth with imperfect bonding is also possible.¹¹ Additionally, since the kinetics of nucleation and growth in CVD-grown MoS₂ is diverse, examining the effects of GBs in large-area polycrystalline samples in different scenarios is essential to fully comprehend their role. Recent reports on the electron transport characteristics of individual grain boundaries in monolayer MoS₂ by examining merged single-crystalline domains have demonstrated some interesting results,¹² but detailed measurements on more diverse sets of grain boundaries and understanding of the underlying scattering mechanisms involved in these GBs remain elusive.

Here, we explore field-effect transport characteristics of CVD-grown MoS₂ with a focus on the role of GBs. We study the field-effect characteristics of polycrystalline large-area MoS₂ films to elucidate the collective role of GBs in the electron transport. To gain insight into these results, we further examine two common MoS₂ GB types and determine that only tilt boundaries have a degrading effect on the MoS₂ electrical transport properties. Through temperature-dependent studies of

the GBs, we explore the mechanisms of charge carrier transport and localizations and provide a comprehensive understanding of the GB related transport characteristics of monolayer MoS₂.

RESULTS

To study the collective effect of GBs on the electrical performance of CVD-grown MoS₂, one must control and quantify the density of line defects. Li *et al.* designed such experiments based on controlling the grain sizes in the films.¹⁷ A systematic control of grain sizes in MoS₂ is not fully developed, and consequently, we introduce two alternative strategies for control of line-defect densities: strategy 1, systematic variation of the line-defect densities in devices with varied channel lengths; strategy 2, stochastic variation of line-defect densities in devices with similar channel lengths. We utilize these two complementary strategies to examine the statistical electrical transport behaviors in polycrystalline samples. For both of these approaches, one needs to develop a line-defect density quantification approach and substantiate the controlled nature of changes in the line-defect densities. A common feature

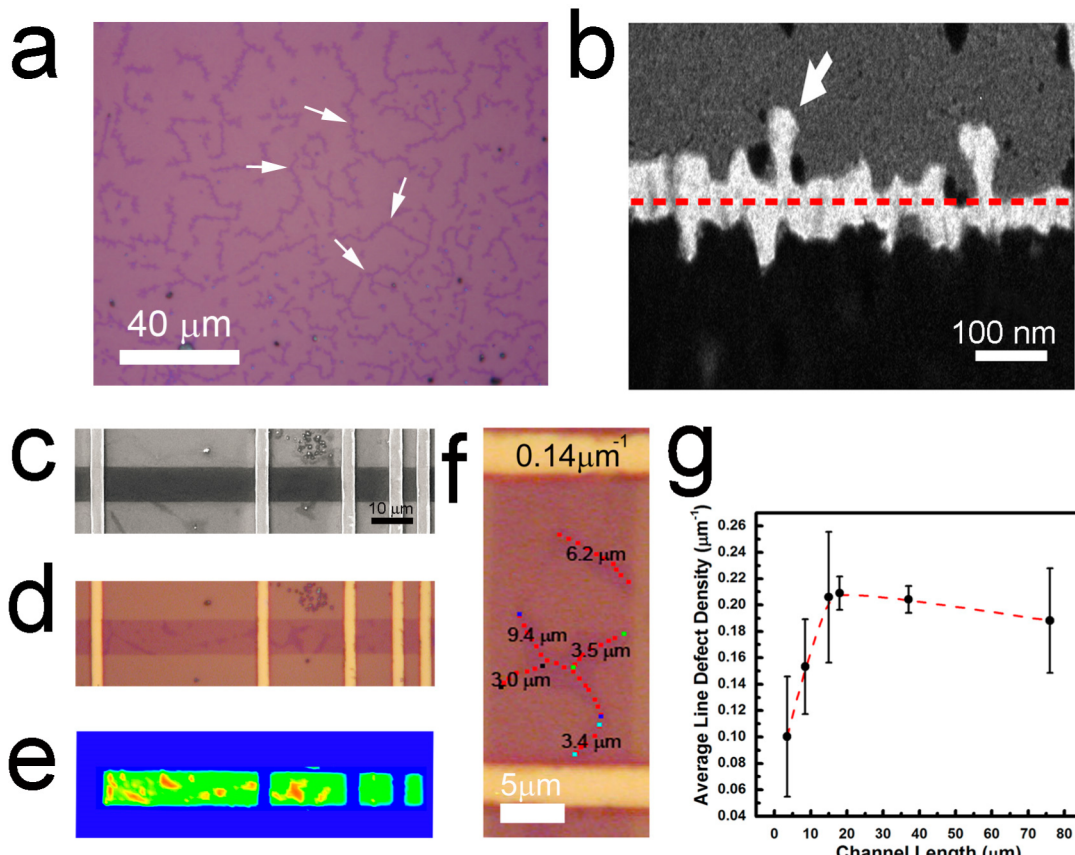


Figure 1. (a) Large-area films suitable for study of collective role of grain boundaries. The arrows highlight instances of overlay growth, commonly seen at grain boundaries. (b) Close examination of secondary layer growth, a common feature of grain boundaries, using dark field transmission electron microscopy. (c, d) The SEM and optical image of the device designed for the channel length dependency measurements. (e) Corresponding Raman map of the same location, showing the distributions of the grain boundaries in the film. (f) We estimate the line defect density by calculating the total length of the bilayered regions ($25.5 \mu\text{m}$ in this example) and dividing by the total channel area ($180 \mu\text{m}^2$ in this example), resulting in a line defect density of $0.14 \mu\text{m}^{-1}$ in the MoS₂ ribbon. (g) The channel length dependency of the estimated line defect density.

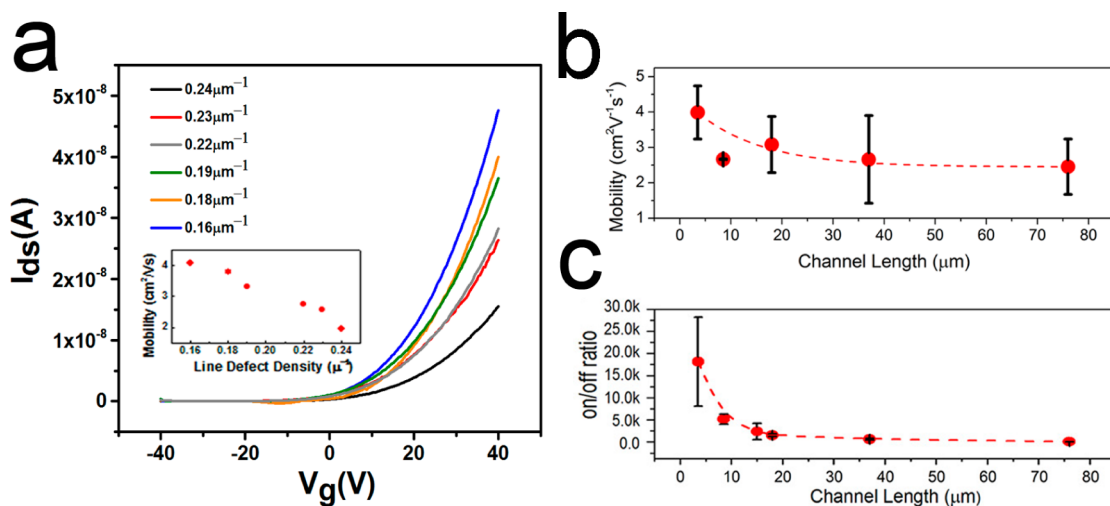


Figure 2. (a) Field-effect characteristics of devices with similar channel length of $18 \mu\text{m}$ but with varied estimated line defect densities containing a variety of randomly oriented and grain boundary types. Inset represents the calculated mobilities for these devices as a function of line defect density. (b, c) Estimated changes in the mobility and on/off ratio of devices as a function of channel length.

of large-area MoS₂ films as confirmed by electron microscopy is the growth of secondary layers along GBs (Figure 1a,b). Many macroscopic tools such as scanning electron, optical, or Raman microscopy can be used to identify these features (Figure 1c–e).¹⁹ Assuming that the formation of secondary layer stripes at the grain boundaries is uniform across the films, one can use this easily quantifiable characteristic as an indirect measure to acquire a rough estimation of line-defect density in the films. We approximate the line-defect density by measuring the total length of these observable line defects, normalized by the total area of their channels (Figure 1f).

For strategy 1, we fabricated seven devices with varied channel lengths and characterized their line defect densities. In each device, the large-area MoS₂ films were patterned into ribbons, and FET transistors with different channel lengths were prepared using conventional photolithography and metallization processes. We observe a systematic change in average line defect density of these devices as a function of channel length as illustrated in Figure 1g. It is evident that the nominal line-defect density increases with the channel length and reaches a saturation level close to $15\text{--}20 \mu\text{m}$ (Figure 1g), which is roughly equal to the estimated grain sizes for the MoS₂ films.¹¹ The results presented in Figure 1g serve as the basis for our study of average GB effects in MoS₂ transport properties.

For strategy 2, we conducted transport measurements on different FET devices with $18\text{-}\mu\text{m}$ -long channel length and varied line defect densities and demonstrated that both mobility and on-state current linearly decreased as a function of the increase in line defect density from 0.16 to $0.24 \mu\text{m}^{-1}$ (Figure 2a). The estimated mobilities in the presented range of line defect densities vary from 4 to $2 \text{ cm}^2/(\text{V s})$ (Figure 2a inset).

Field-effect properties of devices with varied channel lengths showed similar characteristics (Figure 2b). The mobility measurements show an average decrease by roughly 50% as the channel length increases from 3 to $\sim 30 \mu\text{m}$, which corresponds to changes in line-defect density from 0.1 to $0.2 \mu\text{m}^{-1}$. The measurements also show a decrease of roughly 1 order of magnitude in the on/off-current ratios in the same defect density range (Figure 2c). As the channel length increases, the trend of changes in the transport properties closely follow the changes in the line defect density and reaches a plateau region beyond $20 \mu\text{m}$ in channel length where the line-defect density saturates.

It is worth noting that the study of channel length dependence by Liu *et al.* details the short channel effects on the transport properties of single crystal MoS₂.^{20,21} They reveal that, for channel lengths larger than $\sim 1 \mu\text{m}$, the mobility and on/off ratio are expected to saturate at a constant value, as the transport is predominantly in the diffusive regime.^{20,21} Given that the impurity concentration and trapped charges on the substrate are roughly uniform across the channel, it can be deduced that the observed changes in our experiments are largely due to the increased density of line-defects introduced by the GBs. It is known that grain boundaries play an important role as scattering centers that degrade the charge carrier mobility in materials. Previous calculations on the static electronic structures of various grain boundaries in MoS₂ show that the presence of local states deep inside the gap at Mo sites along the grain boundaries act as charge traps that undermine the electronic transport of MoS₂. These scattering centers reduce the mobility of charge carriers in the samples in an expected way while the local changes in the band structure induced by the defects degrade the gating process and reduce

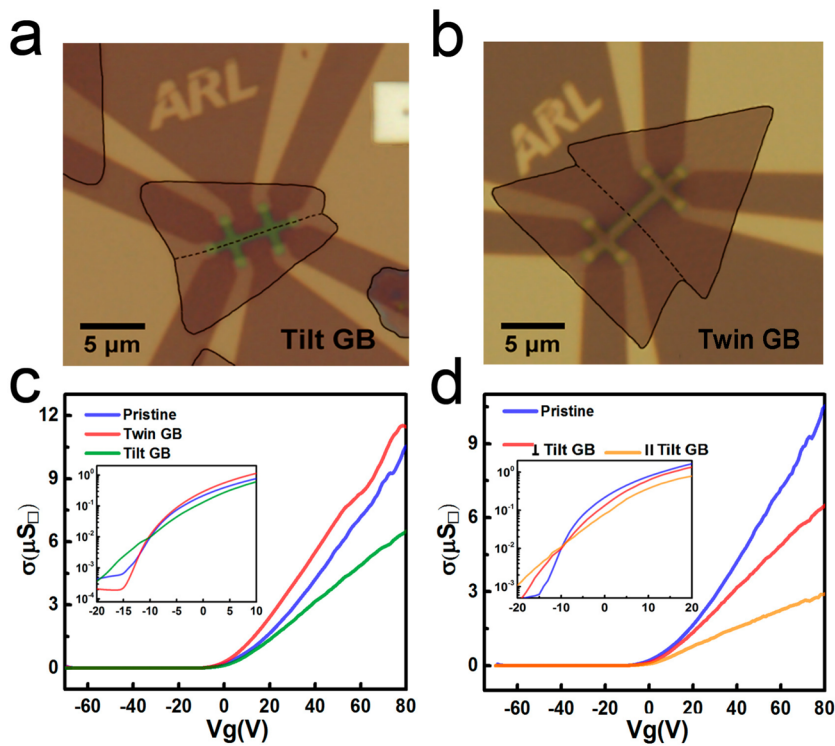


Figure 3. (a, b) Two representative devices for the study of grain boundaries' transport properties. (c) Four-probe electrical transport transfer curves acquired for the devices presented in (a), (b), and pristine MoS₂ samples; inset shows the logarithmic scale of the two types of grain boundaries and pristine curves, demonstrating their relative off-current characteristics. (d) Two probe electrical transport curves for tilt grain boundaries, measured across (\perp) and parallel (\parallel) to the grain boundaries; inset demonstrates their logarithmic-scale, off-current characteristics.

the on/off-current ratio. Additionally, the trapped substrate charges and local interaction variations among the devices are also of high importance, influencing the measured transport properties. However, these measurements are only approximate (although quite indicative) estimations of collective roles played by GBs in large-area samples. In order to obtain more deterministic answer to the underlying mechanisms explaining the role of grain boundaries on electrical transport behaviors, one needs to explore such effects for individual GBs.

Previous studies show that through the regulation of the CVD parameters, the nucleation in MoS₂ monolayers can be controlled to form low density crystals with different relative orientations (separated or merged single-crystal triangles, Figure S1a, Supporting Information).¹¹ This allows for the formation of a variety of samples with different GB types. Accordingly, to acquire a comprehensive knowledge of the GB effects on the electrical transport properties of MoS₂, it is essential to examine these GB variations individually. It is known that two main GB types, tilt and 180° twin, are present in the aggregates of MoS₂ single crystals.^{11–14} However, a variety of these boundaries based on differences in tilt angle and termination elements at the GB are possible. The previous measurements show a slightly higher conductivity and off-current for devices made parallel to the 180° twin

boundaries but almost no change in measurements across the same twin GB.¹² They also demonstrate a decrease in conductivity across the tilt GBs. To better understand the origin of electron scattering in MoS₂ GBs, we first fabricate multiple devices (at least four for each category) that contain only a single GB (Figure 3a,b) and assess their field effect characteristic and electrical transport properties and then compare with devices made on single crystals. In Figure 3a (tilt GB) and 3b (180° twin GB), examples of different MoS₂ GBs examined in our experiments are demonstrated. This GB classification presented here is based on comparisons with similarly merged triangular domains where the GB structure was determined by high resolution transmission microscope characterization.^{11–13} It has been shown that the crystal orientation in each triangular domain is parallel to the triangles' sides.^{11–13} Therefore, the type of GB can be estimated from the domain mismatch angle. However, in this type of analysis, the information about the domain termination atoms cannot be extracted. Nevertheless, our statistical analysis of multiple devices studied in each category reveals two very distinct transport behaviors. The devices made on these samples have a channel width of 1 μm and lengths ranging from 2 to 5 μm. The four-probe conductivity measurements for several devices are shown in Figure 3c. It is clear that tilt GBs are the only type with a significant effect on the electronic

transport of MoS₂. These results show an average four-probe field-effect electron mobility of $12.1 \pm 2.1 \text{ cm}^2/(\text{V s})$ and $6 \pm 1.1 \text{ cm}^2/(\text{V s})$ for pristine single crystalline samples and samples with tilt GBs, respectively. This demonstrates a reduction in field-effect mobility by half in the presence of the tilt GBs. In contrast, the devices made on 180° twin GBs show little or no adverse effect on electrical transport behaviors of MoS₂. A closer look at the off-current and the threshold gating voltages for these GBs also shows a behavior similar to the pristine samples (Figure 3c inset), indicating negligible doping effects in the materials as a result of the GBs. Since tilt GBs seem to play a more important role in influencing the transport property, we then take a closer look at their behaviors.

We perform two-probe transport experiments to investigate the electron-transport behaviors across and parallel to the tilt boundaries in order to delve into the underlying physics of such GBs. The measurements for the two representative devices as compared to pristine samples are presented in Figure 3d. Electron transport parallel to the tilt boundaries is more influenced by the scattering effects than electron transport across them. Our two-probe measurements on multiple devices from each type shows that the average charge carrier field effect mobilities are $4.2 \pm 0.9 \text{ cm}^2/(\text{V s})$ and $2.0 \pm 0.2 \text{ cm}^2/(\text{V s})$ for transport across and along tilt GB, respectively, as compared to $5.8 \pm 0.3 \text{ cm}^2/(\text{V s})$ in the pristine samples. To explain the observed behaviors, one could immediately refer to the intrinsic scattering properties of GBs related to the changes in the lattice potential as electrons move from one grain to the other across the GB. However, this would not explain the behavior of those devices made on parallel directions to GBs in which two parallel conducting channels in each grain could exist. It is also hard to imagine that a line of atomic defects parallel to a conductive channel could dominate the charge carrier transport in a device with a 1 μm wide channel. This is why we hypothesize that the observed effects could be a result of intrinsic and extrinsic scattering centers accumulated at the tilt GBs. Next, we will provide further evidence to prove our hypothesis and identify the sources of such effects.

The examination of the off-current characteristic of the devices made on varied orientations relative to tilt GBs, shown in the inset of Figure 3d in logarithmic scale, indicates that the threshold gate voltage decreases from pristine MoS₂ to samples with tilt GBs. We measure a gate threshold voltage of 10.3 ± 1.9 , 2.5 ± 2.2 , and $-4.0 \pm 2.7 \text{ V}$ for devices made on pristine, across, and along the tilt GBs, respectively. This behavior suggests an increase in n-type charge carriers in MoS₂ samples containing tilt GBs, more so in the devices made parallel to them. One can estimate the changes in doping levels using $n = \varepsilon_0 \varepsilon_r \Delta V_T / te$, where ε_0 and ε_r are the permittivities of free space ($8.85 \times 10^{-12} \text{ F/m}$) and SiO₂ (3.9), respectively; ΔV_T is the difference between

the average threshold voltage measured in pristine and GB included devices, e is the electron charge $1.6 \times 10^{-19} \text{ C}$, and t is the thickness of SiO₂ layer (285 nm). The average increases in doping levels in devices made across and along the tilt GBs as compared to pristine MoS₂ are estimated to be 5.9×10^{11} and $1.1 \times 10^{12} \text{ cm}^{-2}$, respectively. Understanding this observed feature associated with tilt GBs in MoS₂ atomic layers could shed light into their important electronic degradation mechanism for defect engineering in future devices.

The origins of charge carrier types in MoS₂ are an unresolved issue, and the domination of either type of charge carrier has been observed in CVD-grown samples.²² It is known that the sulfur vacancies in this material result in deep midgap donor states below the conduction band.^{13,23} This may be an explanation for both the nature of electronic transport degradation and the doping levels seen in these samples. To further confirm this, we examine the temperature-dependent transport behavior in these samples. The results summarized in Figure 4a–c can be used to identify the nature of electronic states and the role of tilt GBs. It is evident from the temperature dependency of carrier mobilities that the transport is dominated by hopping mechanism and mobility decreases at low temperatures. We plot the conductivity as a function of temperature using the following relationship

$$\sigma = \sigma_0(T) \exp[-(T_0/T)^{1/(d+1)}]$$

where d is the dimensionality and equals 2 in our case, $\sigma_0(T) = AT^m$, where A is constant and $m \sim 0.8\text{--}1$, chosen as 0.8 in our analysis. In all cases, the transport has a general behavior where at low temperatures, below a critical temperature T^* , the conductivity is weakly sensitive to temperature (Figure 4d–f). However, beyond T^* , the conductivity becomes gradually more responsive to temperature changes. Additionally, the changes in charge carrier density through electrostatic gating show a complementary role through screening property changes. The observed behavior is common in highly disordered systems and can be explained by Anderson's model. This approach introduces random potential wells into the periodic potential of the material. The density and depth of these potential wells determine the nature of disorder, and as they are increased, the electronic wave function in the material becomes localized. This localization is strengthened as the density and depth of potential wells are increased. Free electrons are then trapped in these localized states, right below the conduction band. At low temperatures, the electrons do not contribute to the transport and play the role of scattering centers. As the temperature is increased, the electrons can escape these states and contribute to the current in an activated manner. With this picture in mind, one can arrive to a variable range and nearest neighbor

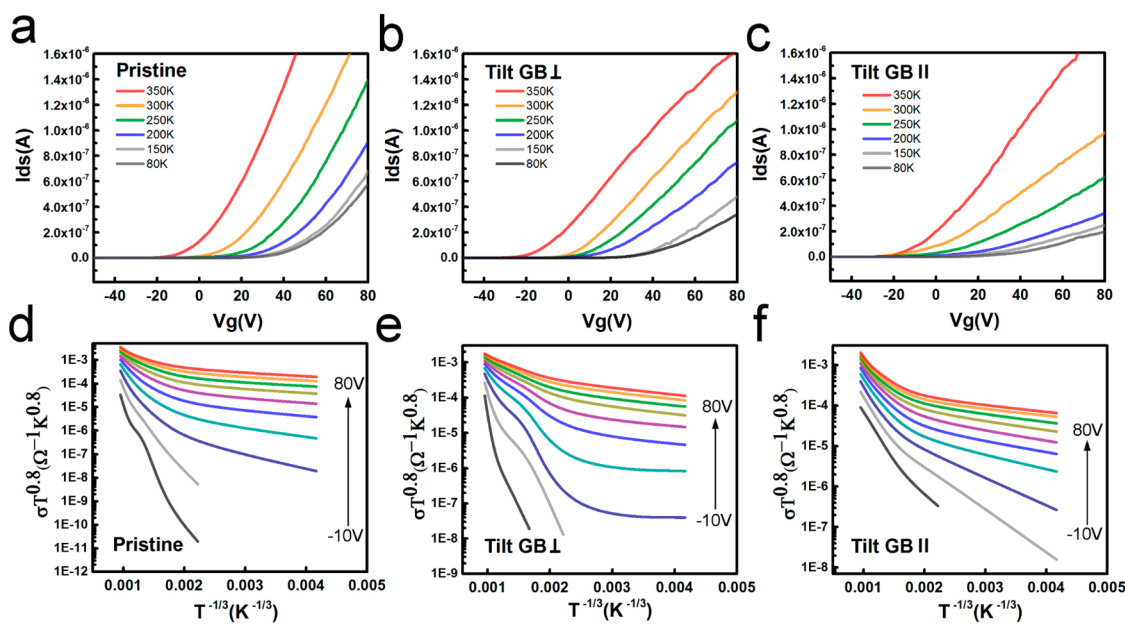


Figure 4. Temperature-dependent field effect characteristics measured using the two-probe configuration of (a) pristine samples, (b) across tilt grain boundaries, (c) along tilt grain boundaries. Gate voltage dependency of activation energy. Temperature dependence of conductivity (σ) and variable range hopping (VRH) at different back gate voltages, measured for (d) pristine, (e) across (\perp) the tilt grain boundary, and (f) parallel (\parallel) to the tilt grain boundaries.

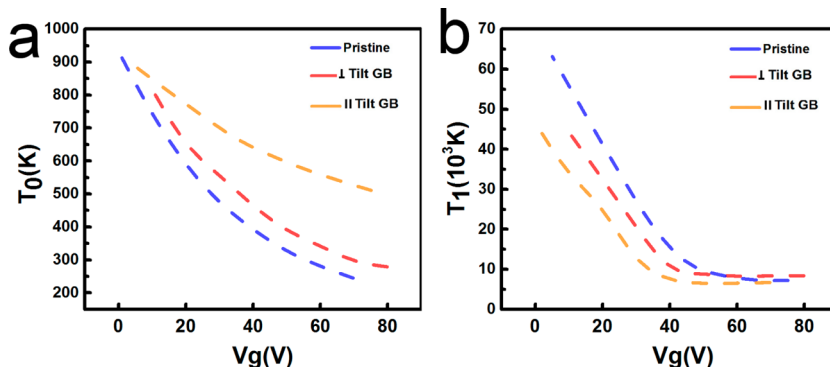


Figure 5. (a) Nearest-neighbor-hopping high-temperature regime temperature coefficient T_0 and its gate voltage dependence. (b) The variable-range-hopping low temperature regime temperature coefficient T_1 and its gate voltage dependence.

hopping transport mechanism for low and high temperature regimes, respectively. The following relationships can be therefore derived to express the temperature dependency of the conductivity σ .

$$T < T^* \quad \sigma \approx \exp[-(T_1/T)^{1/3}]$$

$$T > T^* \quad \sigma \approx \exp(-T_0/T)$$

The two temperature coefficients T_0 and T_1 are important in describing the nature of localized states. Using these relationships one can summarize and express the observations in Figure 4 using the gate voltage dependence of the temperature coefficients (Figure 5). Clearly, as the carrier densities are increased electrostatically, both temperature coefficients decrease. This is because at high charge carrier densities, screening effects mitigate the role of localized states. However, generally a considerable increase in T_0 can be

seen as we move from measurements on pristine samples to samples with devices made perpendicular and parallel to the tilt GBs. The relationship, $K_B T_0 = (N_\mu a^2)^{-1}$ explains the correlation between activation energy and parameters of localization model, where K_B is the Boltzmann constant, N_μ is the density of states at the Fermi energy, and a is the average spacing between potential wells. Assuming a similar density of states at the Fermi level, we can attribute the changes seen between measurements on the GB as compared to pristine samples to the decrease in average spacing of potential wells. This decrease at $V_g = 20$ V translates to an increase in density of potential wells by $\sim 4.9 \times 10^{12} \text{ cm}^{-2}$ and $\sim 1.3 \times 10^{13} \text{ cm}^{-2}$ for vertical and parallel to tilt GB devices as compared to pristine samples, respectively. With this information, we can now focus on understanding the nature of the scattering centers and the random potential wells introduced by them.

Electron microscopy of the mechanically exfoliated samples shows that they typically contain a sufficiently large concentration of sulfur vacancies that can be used to explain the localized and activated transport characteristics in MoS_2 .²³ Several other papers, in contrast, argue that extrinsic substrate doping is of higher importance in terms of charge carrier density and scattering properties in MoS_2 .^{24–27} They demonstrate that the nature of charge carriers in MoS_2 is closely related to the trap states in SiO_2 , which can contribute significantly to the conductivity of the material if they are close to the conduction or valence band. These observations provide two explanations for the sources of doping and scattering in the material. However, in the case of CVD-grown MoS_2 , the density of defects is unsurprisingly higher than samples prepared by exfoliating natural crystals.¹³ If the source of scattering is the sulfur vacancies, then one can only explain the observed behavior by assuming a uniform distribution of sulfur vacancies in the CVD MoS_2 and a higher concentration accumulated at the GBs. This is in agreement with the previous observation of instability and rapid decomposition close to MoS_2 GBs at elevated temperatures (350 K).²⁸ This explanation is also suitable to explain the anomalous behavior observed in devices parallel to the line defects, where, despite the absence of line defects in their direct path, they seem to have an even more prominent effect on the transport. This way, the devices with channels fabricated parallel to the line defects contain higher average densities of point defects as compared to devices made across GBs (Figure S2, Supporting Information). This can be further explored by examining the T_1 gate voltage dependence and its relationship with T_0 . We observe that, as expected, for all configurations, T_1 decreases as V_g is increased. However, the optimum hopping distance results in the following relationship between T_1 and T_0 ²³

$$T_1 = \frac{27T_0}{\pi} \left(\frac{a}{\xi} \right)^2$$

where ξ is the localization length. The average localization length for sulfur vacancies estimated using density functional theory is about 6 Å.²³ Using the values

acquired in Figure 5 and ξ for sulfur vacancies we can estimate the T_1/T_0 ratio to test how the model fits to our experimental results. The calculated T_1/T_0 ratios acquire values 59, 52, and 45 for pristine, across, and along the tilt GBs, respectively. The empirical values extracted from Figure 5 for $V_g = 20$ V are 69, 52, 33, which agree well with the calculated values. As one can see that the small discrepancies between the calculated and experimental results become significantly larger as the charge carrier density is increased at higher V_g . This deviation from the hopping model at higher charge carriers is expected since screening effects mitigate the effects of localized states at higher electrostatic gating. The agreement between the model and empirical results at low gate voltages signifies our hypothesis for accumulation of higher density of point defects at the tilt GBs.

CONCLUSION

In summary, a comprehensive study of the individual and collective role of GBs on the transport properties of MoS_2 atomic layers was discussed. By examining the collective and individual role of line defects in polycrystalline MoS_2 films, we provide additional insights into the role and mechanism of charge carrier scattering. We estimate an average decrease by half in the magnitude of mobility in our devices corresponding to an increase in the line defect density by $0.1 \mu\text{m}^{-1}$. By investigating a variety of GB types, we observe that only tilt GBs have a significant effect on the mobility and transport characteristics of MoS_2 . Further examination of devices made along and across these tilt boundaries reveals an anomalous behavior and a significant level of n-type doping. Low temperature electrical transport measurements confirm a hopping mechanism for electron transport in these samples that can be well explained with Anderson model for disordered systems. From these observations, we conclude that the distinct features in tilt boundaries are more likely caused by accumulation of point defects or other structural defects at these GBs. This comprehensive study illustrates the extent and limitations imposed by GBs in the electronic transport properties of polycrystalline MoS_2 atomic layers.

METHODS

Electron-beam lithography was used to fabricate variable channel length FET and hall bar devices. Photoresist using a MMA/PMMA bilayer resist process was used for all steps. The MoS_2 layer was patterned using a low-power ICP-RIE etch in a CH_4/O_2 plasma, and source and drain contacts were formed via e-beam evaporated Ti/Au (15/85 nm).

Field effect transistor (FET) devices with variable channel lengths are made by photolithography process using LOR5B as an adhesive layer and photoresist S1813, mask aligner (SUSS Mask Aligner MJB4), and O_2 -reactive ion etching (RIE, Phantom III). The photoresist is removed by acetone and PG-REMOVER. The electrodes (Ti/Au, 4 nm/40 nm) are deposited using an e-beam evaporator. All electrical measurements are performed

in a Lakeshore probe station under vacuum conditions ($<10^{-5}$ Torr). These devices were analyzed using either an Agilent B1500A or Keithly 4200 Semiconductor Device Analyzer.

In all measurements, we estimate the charge carrier mobility in these devices using the equation $\mu = [dI_{ds}/dV_{bg}] \cdot [(L/(WC_1V_{ds}))]$, where L and W are the channel length and width. The capacitance between the channel and the back gate per unit area is estimated to be $\sim 1.2 \times 10^{-4} \text{ F m}^{-2}$ ($C_1 = \epsilon_0 \epsilon_r / d$, where $\epsilon_0 = 3.9$ and $d = 285$ nm). The theoretical estimate for the capacitance of SiO_2 will provide us with a lower limit estimate for the calculated mobilities.

Micro-Raman and photoluminescence (PL) measurements were performed with a WITec Alpha 300RA system using the 532 nm line of a frequency-doubled Nd:YAG laser as the excitation source. The spectra were measured in the backscattering

configuration using a 100 \times objective and either a 600 or 1800 grooves/mm grating. The spot size of the laser was \sim 342 nm resulting in an incident laser power density \sim 140 μ W/ μ m 2 . This laser power was found to be sufficiently low to not to cause any shifting in the both the in-plane and out-of-plane modes of the Raman signature.

Conflict of Interest: The authors declare no competing financial interest.

Acknowledgment. This work was supported by the Welch Foundation (Grant No. C-1716), the NSF (Grant No. DMR-1327093), the U.S. Army Research Office (MURI Grant No. W911NF-11-1-0362), the U.S. Office of Naval Research (MURI Grant No. N000014-09-1-1066), and the Nanoelectronics Research Corporation contract S201006. This research was also supported in part by the National Science Foundation through Grant No. DMR-0938330. M.D., M.A., M.L.C., A.G.B., and T.P.O. acknowledge the support of the ARL Director's Strategic Initiative (DSI) program on interfaces in stacked 2D atomic layered materials. The authors would also like to thank Dr. Pani Varanasi, ARO for his in-depth technical discussion on 2D atomic layer R&D. The views and conclusions contained in this document are those of the authors and should not be interpreted as representing the official policies, either expressed or implied, of the ARL or the U.S. Government. This work was also supported by the Singapore National Research Foundation under NRF RF Award No. NRF-RF2013-08, the start-up funding from Nanyang Technological University (M4081137.070).

Supporting Information Available: Raman and PL maps acquired from the grain boundary regions of devices; explanations for the hypothesis about the variations in defect concentrations close to grain boundaries demonstrated through examination of electrical performance of devices made parallel and vertical to the tilt grain boundaries; table summarizing multiple measurements and statistics on different devices to support the conclusions in the main text. This material is available free of charge via the Internet at <http://pubs.acs.org>.

REFERENCES AND NOTES

- Mak, K. F.; Lee, C.; Hone, J.; Shan, J.; Heinz, T. F. Atomically Thin MoS₂: A New Direct-Gap Semiconductor. *Phys. Rev. Lett.* **2010**, *105*, 136805.
- Radisavljevic, B.; Radenovic, A.; Brivio, J.; Giacometti, V.; Kis, A. Single-Layer MoS₂ Transistors. *Nat. Nano* **2011**, *6*, 147–150.
- Behnia, K. Condensed-Matter Physics: Polarized Light Boosts Valleytronics. *Nat. Nano* **2012**, *7*, 488–489.
- Cao, T.; Wang, G.; Han, W.; Ye, H.; Zhu, C.; Shi, J.; Niu, Q.; Tan, P.; Wang, E.; Liu, B.; Feng, J. Valley-Selective Circular Dichroism of Monolayer Molybdenum Disulphide. *Nat. Commun.* **2012**, *3*, 887.
- Mak, K. F.; He, K.; Shan, J.; Heinz, T. F. Control of Valley Polarization in Monolayer MoS₂ by Optical Helicity. *Nat. Nano* **2012**, *7*, 494–498.
- Zeng, H.; Dai, J.; Yao, W.; Xiao, D.; Cui, X. Valley Polarization in MoS₂ Monolayers by Optical Pumping. *Nat. Nano* **2012**, *7*, 490–493.
- Zhu, Z. Y.; Cheng, Y. C.; Schwingenschlögl, U. Giant Spin-Orbit-Induced Spin Splitting in Two-Dimensional Transition-Metal Dichalcogenide Semiconductors. *Phys. Rev. B* **2011**, *84*, 153402.
- Zhan, Y.; Liu, Z.; Najmaei, S.; Ajayan, P. M.; Lou, J. Large-Area Vapor-Phase Growth and Characterization of MoS₂ Atomic Layers on a SiO₂ Substrate. *Small* **2012**, *8*, 966–971.
- Liu, K.-K.; Zhang, W.; Lee, Y.-H.; Lin, Y.-C.; Chang, M.-T.; Su, C.-Y.; Chang, C.-S.; Li, H.; Shi, Y.; Zhang, H.; et al. Growth of Large-Area and Highly Crystalline MoS₂ Thin Layers on Insulating Substrates. *Nano Lett.* **2012**, *12*, 1538–1544.
- Lee, Y.-H.; Zhang, X.-Q.; Zhang, W.; Chang, M.-T.; Lin, C.-T.; Chang, K.-D.; Yu, Y.-C.; Wang, J. T.-W.; Chang, C.-S.; Li, L.-J.; et al. Synthesis of Large-Area MoS₂ Atomic Layers with Chemical Vapor Deposition. *Adv. Mater.* **2012**, *24*, 2320–2325.
- Najmaei, S.; Liu, Z.; Zhou, W.; Zou, X.; Shi, G.; Lei, S.; Yakobson, B. I.; Idrobo, J.-C.; Ajayan, P. M.; Lou, J. Vapour Phase Growth and Grain Boundary Structure of Molybdenum Disulphide Atomic Layers. *Nat. Mater.* **2013**, *12*, 754–759.
- van der Zande, A. M.; Huang, P. Y.; Chenet, D. A.; Berkelbach, T. C.; You, Y.; Lee, G.-H.; Heinz, T. F.; Reichman, D. R.; Muller, D. A.; Hone, J. C. Grains and Grain Boundaries in Highly Crystalline Monolayer Molybdenum Disulphide. *Nat. Mater.* **2013**, *12*, 554–561.
- Zhou, W.; Zou, X.; Najmaei, S.; Liu, Z.; Shi, Y.; Kong, J.; Lou, J.; Ajayan, P. M.; Yakobson, B. I.; Idrobo, J.-C. Intrinsic Structural Defects in Monolayer Molybdenum Disulfide. *Nano Lett.* **2013**, *13*, 2615–2622.
- Zou, X.; Liu, Y.; Yakobson, B. I. Predicting Dislocations and Grain Boundaries in Two-Dimensional Metal-Disulfides from the First Principles. *Nano Lett.* **2012**, *13*, 253–258.
- Yazyev, O. V.; Louie, S. G. Electronic Transport in Polycrystalline Graphene. *Nat. Mater.* **2010**, *9*, 806–809.
- Liu, Y.; Zou, X.; Yakobson, B. I. Dislocations and Grain Boundaries in Two-Dimensional Boron Nitride. *ACS Nano* **2012**, *6*, 7053–7058.
- Li, X.; Magnuson, C. W.; Venugopal, A.; An, J.; Suk, J. W.; Han, B.; Borysiak, M.; Cai, W.; Velamakanni, A.; Zhu, Y.; et al. Graphene Films with Large Domain Size by a Two-Step Chemical Vapor Deposition Process. *Nano Lett.* **2010**, *10*, 4328–4334.
- Tsen, A. W.; Brown, L.; Levendorf, M. P.; Ghahari, F.; Huang, P. Y.; Havener, R. W.; Ruiz-Vargas, C. S.; Muller, D. A.; Kim, P.; Park, J. Tailoring Electrical Transport Across Grain Boundaries in Polycrystalline Graphene. *Science* **2012**, *336*, 1143–1146.
- Lee, C.; Yan, H.; Brus, L. E.; Heinz, T. F.; Hone, J.; Ryu, S. Anomalous Lattice Vibrations of Single- and Few-Layer MoS₂. *ACS Nano* **2010**, *4*, 2695–2700.
- Liu, H.; Neal, A. T.; Ye, P. D. Channel Length Scaling of MoS₂MOSFETs. *ACS Nano* **2012**, *6*, 8563–8569.
- Liu, H.; Si, M.; Najmaei, S.; Neal, A. T.; Du, Y.; Ajayan, P. M.; Lou, J.; Ye, P. D. Statistical Study of Deep Submicron Dual-Gated Field-Effect Transistors on Monolayer Chemical Vapor Deposition Molybdenum Disulfide Films. *Nano Lett.* **2013**, *13*, 2640–2646.
- Dolui, K.; Rungger, I.; Sanvito, S. Origin of the n-Type and p-Type Conductivity of MoS₂ Monolayers on a SiO₂ Substrate. *Phys. Rev. B* **2013**, *87*, 165402.
- Qiu, H.; Xu, T.; Wang, Z.; Ren, W.; Nan, H.; Ni, Z.; Chen, Q.; Yuan, S.; Miao, F.; Song, F.; et al. Hopping Transport Through Defect-Induced Localized States in Molybdenum Disulphide. *Nat. Commun.* **2013**, *4*.
- Ayari, A.; Cobas, E.; Ogundadegbe, O.; Fuhrer, M. S. Realization and Electrical Characterization of Ultrathin Crystals of Layered Transition-Metal Dichalcogenides. *J. Appl. Phys.* **2007**, *101*, 014507–5.
- Jariwala, D.; Sangwan, V. K.; Late, D. J.; Johns, J. E.; Dravid, V. P.; Marks, T. J.; Lauhon, L. J.; Hersam, M. C. Band-Like Transport in High Mobility Unencapsulated Single-Layer MoS₂ Transistors. *Appl. Phys. Lett.* **2013**, *102*.
- Ghatak, S.; Pal, A. N.; Ghosh, A. Nature of Electronic States in Atomically Thin MoS₂ Field-Effect Transistors. *ACS Nano* **2011**, *5*, 7707–7712.
- Radisavljevic, B.; Kis, A. Mobility Engineering and a Metal–Insulator Transition in Monolayer MoS₂. *Nat. Mater.* **2013**, *12*, 815–820.
- Najmaei, S.; Ajayan, P. M.; Lou, J. Quantitative Analysis of the Temperature Dependency in Raman Active Vibrational Modes of Molybdenum Disulfide Atomic Layers. *Nano-scale* **2013**, *5*, 9758–9763.